ECCOMAS Congress 2016
VII European Congress on Computational Methods in Applied Sciences and Engineering
M. Papadrakakis, V. Papadopoulos, G. Stefanou, V. Plevris (eds.)
Crete Island, Greece, 5–10 June 2016

A TWO-LEVEL HYBRID APPROACH FOR OPTIMAL ACTIVE FLOW CONTROL ON A THREE-ELEMENT AIRFOIL

Anil Nemili[1], Emre Özkaya[2], Nicolas R. Gauger[2], Felix Kramer[3] and Frank Thiele[3]

[1]Department of Mathematics, BITS Pilani - Hyderabad Campus, Hyderabad 500078, India
e-mail: anil@hyderabad.bits-pilani.ac.in

[2] Chair for Scientific Computing, Technische Universität Kaiserslautern, 67663 Kaiserslautern, Germany
e-mail: {emre.oezkaya, nicolas.gauger}@scicomp.uni-kl.de

[3] CFD Software Entwicklungs- und Forschungsgesellschaft mbH, 10625 Berlin, Germany
e-mail: {felix.kramer, frank.thiele}@cfd-berlin.com

Keywords: Active Flow Control, Unsteady RANS, Hybrid optimization, Discrete adjoints, Evolutionary Algorithms, Algorithmic Differentiation, Multi-element airfoil

Abstract. *In this paper we present a two-level approach that combines an adjoint-based gradient search method with an evolutionary algorithm for optimal active flow control. The suggested method effectively combines the advantages of both approaches and achieves a good compromise between the computational effort and the degree of freedom used in optimization. In the first level, a global optimization is performed with few design parameters using an evolutionary algorithm. In the second level, the global optimal solution from the first level is taken as the initial setting for the adjoint based local optimization using a large number of design parameters. The unsteady discrete adjoint solver required for the second level is developed based on Algorithmic Differentiation techniques for the unsteady incompressible flowsgoverned by Unsteady Reynolds-Averaged Navier Stokes (URANS) equations. In this way, the discrete adjoint solver is robust and has exactly the same functionality with the underlying URANS flow solver. The applicability of the two-level method is demonstrated by finding the optimal parameters of the active flow control mechanism on a three element airfoil configuration at a Reynolds number of* $Re = 10^6$ *and an angle of attack of* $AoA = 6^\circ$*. Numerical results have shown that the hybrid approach completely suppressed the separation and very significantly increased the mean-lift coefficient by* 67% *compared to the un-actuated baseline flow.*

1 INTRODUCTION

Application of active flow control methods [1] to delay the flow separation on the flap of modern transport aircraft has been the subject of research for many years. An active flow control technique that is of particular interest to us is the predetermined or the so-called open-loop active flow control approach. Typically, these methods supply energy or auxiliary power to the boundary layer through an actuator. The additional longitudinal momentum due to actuation delays or even completely suppresses the flow separation. Various researchers have performed several experimental [2, 3, 4, 5, 6] and numerical investigations [7, 8, 9] to study the effect of actuation in delaying the separation on the flap and enhancing the overall aerodynamic performance of high-lift configurations. In the present work, synthetic jets, also known as zero-net-mass-flux actuators [10, 11] are employed to control the flow separation on the suction side of the flap. Common parameters of these actuators are amplitude, blowing angles, frequency and the phase shift between two adjacent actuators. Effective separation control and thus delaying aerodynamic stall to enhance maximum lift can be achieved by finding the optimal set of actuation parameters.

The optimal values of the actuation parameters can be efficiently determined by employing gradient-based optimization algorithms combined with adjoint approaches. A nice feature of the adjoint approaches is that they enable the evaluation of gradient vectors at a fixed computational effort. Therefore, optimization studies with a higher degree of freedom become viable and better control mechanisms can be achieved. Broadly, we can classify the adjoint approaches into continuous and discrete adjoint methods. In the continuous adjoint method [12, 13], one first derives the optimality system from the continuous optimization problem and the resulting adjoint partial differential equations (PDEs) are then discretised and solved using numerical methods. Although being computationally efficient, development of continuous adjoint flow solvers requires much effort and their maintenance becomes a problem as the underlying non-linear flow solvers are subject to continuous modifications, e.g., new boundary conditions, new turbulence models etc. On the other hand, in the discrete adjoint method, one first discretizes the state PDEs that govern the fluid flow, and then derives the discrete adjoint equation based on the optimization problem in discrete form. In general, discrete adjoint solvers are more straightforward to implement, and therefore they have found a wider acceptance for the applications of practical relevance.

In general, a discrete adjoint solver for optimal active flow control can be developed either by using the so-called hand-discrete approach [14] or by employing Algorithmic Differentiation (AD) techniques [15, 16]. In the hand-discrete approach, the governing flow equations are first discretized as usual. The adjoint equations are then derived by linearizing various terms, which comprise the discrete cell residuals. These terms involve convective and viscous fluxes as well as source terms. Finally a computer code is implemented to solve the unsteady adjoint equations and to compute the design sensitivities using the adjoint solution. On the other hand, in the AD based approach the adjoint code is generated by applying AD techniques [17] directly to the source code of the corresponding flow solver.

Accurate computation of sensitivity information requires exact differentiation of all residual terms in discretized state equations. However, the exact linearization of all terms in the discrete residual is quite complex, laborious and might be often prone to errors. To simplify this tedious

effort and ease the development of the adjoint solvers, various Jacobian approximations [18] have been proposed in the past. In these approximations, linearization of certain terms in the flux Jacobian is omitted. Examples of these are, turbulent models, flux limiters, reconstruction operator for higher order accuracy, model parameters of the convective schemes etc. Jacobian approximations may result in inaccurate computation of sensitivities [19]. In fact, in unsteady flows, the effect of these approximations on the accuracy of sensitivities is much more significant as the errors generated in the adjoint solution tend to accumulate rapidly while solving the adjoint equations backward-in-time [16]. On the other hand, using the AD techniques the exact differentiation of all residual terms can be performed with much ease.

Although being computationally very efficient, adjoint-based gradient search methods may perform poorly in some cases as their solutions tend to be trapped to local optima. In problems with fairly noisy response surfaces, it is typical that the optimization method yields some improvement after few cycles. However, further cycles may not yield any significant improvement. Moreover, gradient-based algorithms are highly sensitive to the initial values chosen for the design parameters. Therefore, a "bad" initial setting for the design parameters may result in a significantly lower performance than expected. As a remedy to this problem, a global optimization method may provide a better improvement within a specified design space. For example, Evolutionary Algorithms (EAs) [20, 21], which try to imitate the natural evolution processes, are widely accepted as global optimization tools. EAs are generally computationally expensive and require a prohibitive amount of computational resources if the number of design parameters is large. For this reason, EAs are applicable to limited problems with a few design variables and they are usually implemented in conjunction with surrogate modeling techniques such as response surface methods [22], radial basis functions [23] or Kriging method [24].

In the present study, an efficient two-level design strategy is employed by taking advantage of both the global optimization method based on EA and the local optimization from the adjoint-based gradient search. Since very few design parameters are used in the first level, the evolutionary algorithm is constructed directly based on the non-linear URANS simulations. In the second level, a gradient-based optimization is started using the best initial values provided by the global optimization from the first level. In order to fully exploit the capabilities of the adjoint solver, the control parameters of the actuation are allowed to vary spatially in the flap region so that largest degree of freedom is taken for the optimization, thus allowing the maximum design space dimension. A similar design strategy for aerodynamic shape optimization is suggested in [25].

This paper is organized as follows. Section 2 is devoted to the development of a robust and accurate discrete adjoint incompressible URANS solver, meant for optimal active flow control. In Section 3, we present the EA based optimization method, which is employed to specify the initial point for the gradient-based optimization stage. In Section 4, we introduce the configuration used in the present study along with the features of flow and adjoint solvers used in the present work. In Section 5, numerical results are presented based on optimal synthetic jet actuation on the three-element airfoil high-lift configuration. Finally, conclusions are drawn in Section 6.

2 A DISCRETE ADJOINT APPROACH FOR OPTIMAL ACTIVE FLOW CONTROL

Consider the problem of finding an optimal active flow control mechanism that delays or suppresses the flow separation and thus increases the stall angle of the three-element airfoil. This amounts to the solution of a PDE-constrained optimal control problem. Since we are interested in enhancing the overall lift coefficient, the objective function is defined as the time-averaged lift coefficient. The PDE constraints are the incompressible URANS equations, that govern the low speed flows during the landing and take-off phases of modern transport aircraft. The control variables are the parameters of actuation.

In the discrete form, the time-averaged or the mean lift coefficient $\overline{C}_l$ over the time interval $[0, T]$ can be defined as

$$\overline{C}_l = \frac{1}{N} \sum_{n=1}^{N} I^n \left(\mathbf{U}^n, \alpha \right), \quad I^n = C_l^n \tag{1}$$

where $\mathbf{U}^n$ and C_l^n are the state vector and the lift coefficient at time iteration n respectively. α is the vector of control variables comprising the actuation parameters amplitude, frequency, phase shift and blowing angle. $N = T/\Delta t$ is the number of time iterations that span the given time interval and Δt is the step size of the time discretisation scheme. At each time iteration n, the discretised URANS equations are solved for the solution of the state vector $\mathbf{U^n}$ by a contractive fixed-point iterative scheme of the form

$$\mathbf{U}_{i+1}^n = G^n \left(\mathbf{U}_i^n, \mathbf{U}^{n-1}, \mathbf{U}^{n-2}, \alpha \right), \; n = 1, \ldots, N. \tag{2}$$

Here, G^n represents an iteration of the pressure-velocity coupling scheme based on the SIMPLE algorithm, employed for solving the incompressible URANS equations. $\mathbf{U}^{n-1}$ and $\mathbf{U}^{n-2}$ are the converged state vectors at time iterations $n-1$ and $n-2$ respectively. Note that the transient terms in the governing equations are approximated by a second-order implicit backward difference formula. The Lagrangian associated with the constrained optimization problem given by Eqs. (1) and (2) is defined as

$$L = \frac{1}{N} \sum_{n=1}^{N} \left\{ I^n \left(\mathbf{U}^n, \alpha \right) \right\} - \sum_{n=1}^{N} \left\{ \left(\overline{\mathbf{U}}^n \right)^T \left(\mathbf{U}^n - G^n \left(\mathbf{U}^n, \mathbf{U}^{n-1}, \mathbf{U}^{n-2}, \alpha \right) \right) \right\}, \tag{3}$$

where $\overline{\mathbf{U}}^n$ is the vector of Lagrangian multipliers or the adjoint state vector at time iteration n. From the first order necessary conditions for optimality (KKT conditions), the discrete adjoint URANS equations can be derived in the fixed-point form as

$$\overline{\mathbf{U}}_{i+1}^n = \left[\frac{\partial G^n}{\partial \mathbf{U}^n} \right]^T \overline{\mathbf{U}}_i^n + \left[\frac{\partial G^{n+1}}{\partial \mathbf{U}^n} \right]^T \overline{\mathbf{U}}^{n+1} + \left[\frac{\partial G^{n+2}}{\partial \mathbf{U}^n} \right]^T \overline{\mathbf{U}}^{n+2} + \frac{1}{N} \left[\frac{\partial I^n}{\partial \mathbf{U}^n} \right]^T. \tag{4}$$

Here, $\overline{\mathbf{U}}^{n+1}$ and $\overline{\mathbf{U}}^{n+2}$ are the converged adjoint solutions at time iterations $n+1$ and $n+2$ respectively. Unlike the flow equations, the adjoint equations are solved backward-in-time starting from $n = N$ to $n = 1$. The solution of the adjoint equations is then used to compute the actuation sensitivities as

$$\frac{dL}{d\alpha} = \sum_{n=1}^{N} \left\{ \frac{1}{N} \frac{\partial I^n}{\partial \alpha} + \left(\overline{\mathbf{U}}^n \right)^T \frac{\partial G^n}{\partial \alpha} \right\}. \tag{5}$$

From Eqs. (4) and (5) it can be observed that an accurate computation of actuation sensitivities requires the exact differentiation of the I^n and G^n. Note that the fixed-point iterator G^n consists of residuals due to turbulence models, higher-order convective scheme and terms related to implicit time marching algorithm. The exact differentiation of these terms by hand is laborious and prone to errors. On the other hand, Algorithmic Differentiation techniques [17] can be used to perform the exact differentiation of G^n with much ease. Since all terms in the fixed-point iterator can be differentiated exactly, the adjoint code based on AD computes sensitivities that are always accurate and consistent to the solutions obtained by URANS simulations. Furthermore, the adjoint solver inherits the robustness and the asymptotic rate of convergence of the underlying URANS solver [17]. The ability of the AD based approach in accurate computation of sensitivities in incompressible URANS simulations is successfully demonstrated on practical configurations [26].

3 AN EVOLUTIONARY ALGORITHM FOR THE INITIAL CONTROL

Since the results obtained from gradient search algorithms are highly sensitive to the starting values of the actuation parameters, the initial values chosen for these parameters play a crucial role on the success of the optimization study. In general, values obtained from previous simulations and/or experimental results can be specified for the initial values of the actuation parameters. These values are, however, likely to be far away from the optimal values. If initially the actuation parameters are not allowed to vary spatially, application of an EA based optimization using direct URANS simulations is viable since in this case the design vector has only four parameters, namely amplitude, frequency, phase shift of the actuation and the angle of blowing/suction. The evolutionary algorithm used in this work includes the following basic ingredients:

- Selection of the initial sample points using the Latin Hypercube Sampling (LHS) method.
- URANS simulations at the initial sample points to form an initial population for the EA.
- Selection of a parent pair for the reproduction process based on the fitness values of each member in the population.
- The cross-over process between the parent designs using random Gaussian distribution to determine the design parameters of the children (new designs).
- URANS simulation performed at each new design.
- Removal of the member with the worst fitness from the population in each 10 iterations.

The initial population used for the EA algorithm is formed using the LHS method obtained with initial URANS simulations. The selection of the parent pair for the reproduction step is performed by a randomized selection procedure using a roulette wheel containing reproduction likelihoods of each member in the population. The cross-over process between the parent members are then performed using random Gaussian distributions with a mutation likelihood close to 5% (chosen to be 2σ event). As an example, in Figure 1, the probability distribution function obtained by random 10^7 realizations of a cross-over process between two designs with $x = 1.0$ and $x = 5.0$ is shown. As one may notice, the majority of the designs (close to 95%) lie between 1.0 and 5.0. Only a small amount of new designs lie outside this range (in shaded

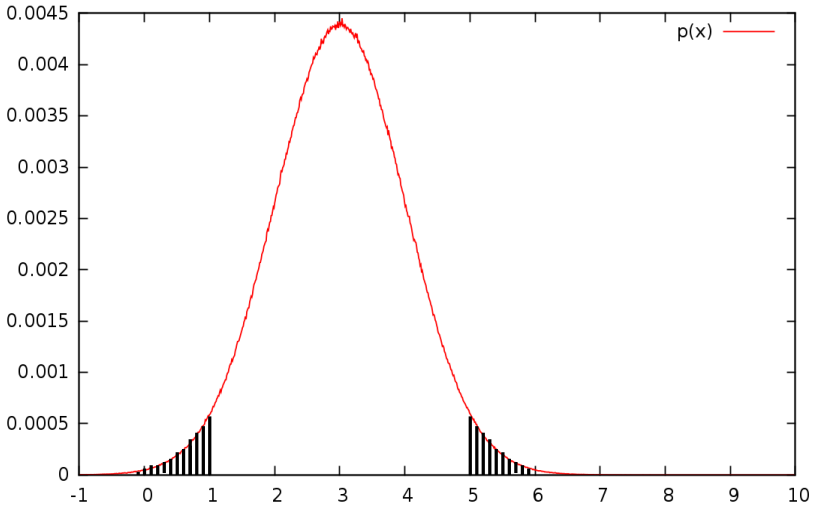

Figure 1: Gaussian distribution of new designs for $x_1 = 1.0$ and $x_2 = 5.0$ obtained from 10^7 different cross-overs.

area). These designs are considered as a result of mutations.

Once the new design point is determined as a result of the cross-over process, a new URANS simulation is performed at this design point and the fitness values of the population members and the reproduction likelihoods of each member in the population (roulette wheel) are accordingly adjusted. After every 10 reproductions, one member with the worst fitness value is removed from the population. The stopping criteria in the EA based optimization is specified as the maximum number of URANS simulations and is set to 250. Therefore, the global optimization in the first level terminates after 250 iterations. The global optimum result obtained by the global optimization is then used to specify the initial values for the actuation parameters in the gradient-search optimization. In contrast to the first level, in the second level, the actuation parameters are allowed to vary in each actuation slot. Therefore, the dimension of the design vector increases from 4 to 162. In Figure 2, the two-level approach is illustrated schematically.

4 COMPUTATIONAL SETUP

4.1 Configuration Details

The geometry of the three-element high-lift configuration is shown in Figure 3. The high-lift configuration consists of a main airfoil with extended slat and flap. The relative chord lengths of slat and flap are given by $l_{slat} = 0.158l_c$ and $l_{flap} = 0.254l_c$, where l_c is the chord length. The flap deflection angle is set to $\delta_{flap} = 37^o$ while the angle of attack is fixed at $AoA = 6^o$. This angle of attack is within the typical range of angle of attack during landing scenarios of modern commercial aircraft. It may be noted that with these settings, the flow over the flap is detached from the shoulder region, while the flow over the slat and main airfoil is still fully attached. Therefore, the above settings are best suited for the application of an active flow control mechanism to delay the separation on the suction side of the flap.

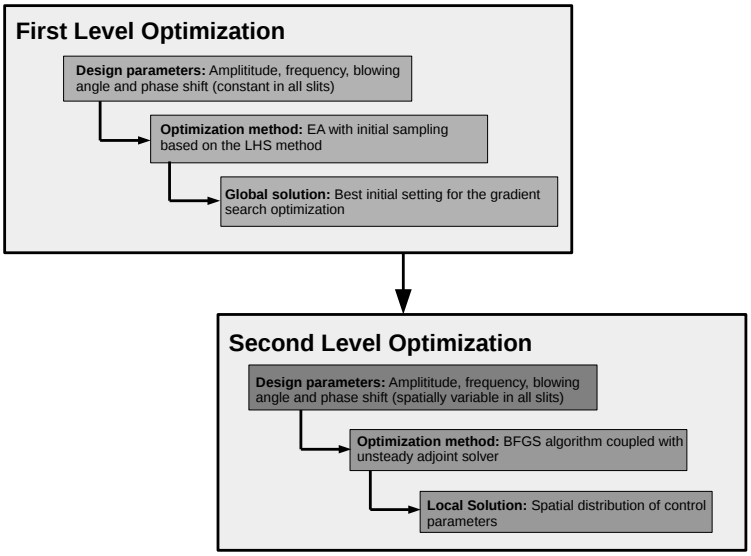

Figure 2: Illustration of the two-level method for optimal active flow control on a three-element airfoil.

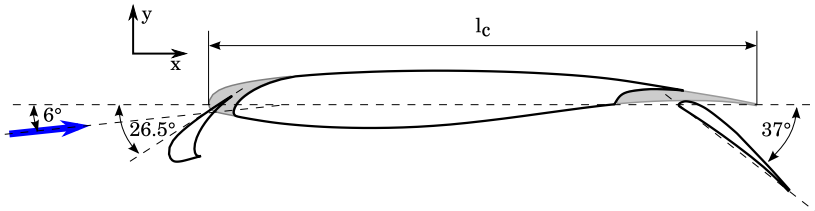

Figure 3: Sketch of a three-element airfoil high-lift configuration.

4.2 Computational Domain

The computational domain consists of a block-structured grid with $172,392$ finite volumes. Figure (4) shows the grid around the flap of the high-lift configuration. The flap boundary has 370 grid points. Note that the non-dimensional wall distance of the first cell center remains below $y^+ = 1$ on the entire surface.

4.3 Boundary Conditions

At the inlet boundary all flow quantities are prescribed. At the outflow, a convective boundary condition is used that allows unsteady flow structures to be transported outside the domain. On the airfoil-flap-slat surface no-slip boundary condition is used. In the present work, the flow control is realized by applying synthetic jet actuation at 27 slots on the suction side of the flap, as shown in Figure (5). Numerically, each slot is resolved by two cell faces on the flap boundary. It can be observed that the actuation is distributed almost on the entire flap starting from the shoulder region. The actuation boundary condition at a flap face is defined by

$$\begin{pmatrix} u \\ v \end{pmatrix} = A \cdot u_\infty \begin{pmatrix} \frac{\cos\theta}{\tan\beta} - \sin\theta \\ \frac{\sin\theta}{\tan\beta} + \cos\theta \end{pmatrix} \sin[2\pi F \cdot (t - t_0)] \tag{6}$$

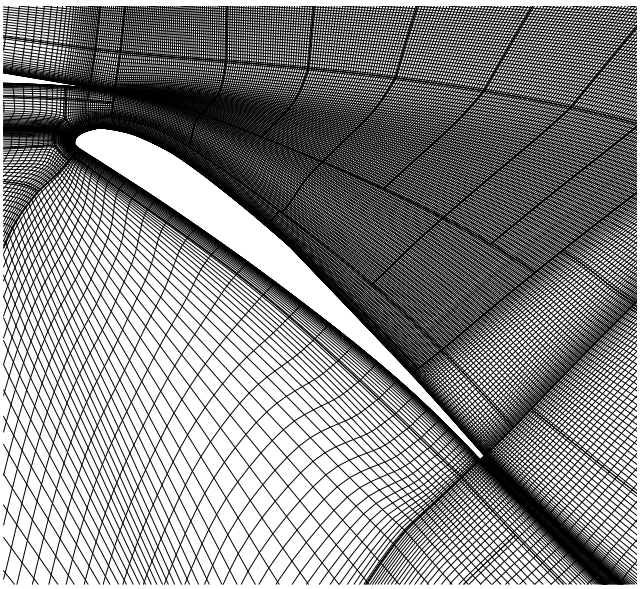

Figure 4: Block-structured grid around the flap of a three-element airfoil.

Here u and v are components of the actuation velocity vector, A is the non-dimensional amplitude of actuation, u_∞ is the free-stream velocity, β is the blowing angle, F is the non-dimensional frequency, t is the non-dimensional physical time and t_0 is the non-dimensional phase shift. The angle of the slit face, θ is fixed by the geometry of the airfoil. The named quantities are appropriately non-dimensionalised by u_∞.

4.4 Numerical Solvers

In the present work, the URANS calculations are performed using the multi-purpose parallel CFD code ELAN [7, 8]. ELAN is an incompressible finite volume solver based on the SIMPLE algorithm. The code is fully implicit and is of second order accuracy both in space and time. The convective fluxes are approximated by a total variation diminishing (TVD) scheme. In addition, the code offers various options for RANS/LES turbulence models.

The discrete adjoint URANS code ELAN-A [16, 26] is developed by applying the AD tool Tapenade [27] to the underlying URANS solver. ELAN-A retains all features of the ELAN code.

5 RESULTS AND DISCUSSION

In this section, we present the numerical results based on optimal active flow control mechanism on the three-element airfoil high-lift configuration. We first consider the base flow without actuation. The incompressible URANS simulations are performed with the SST $k-\omega$ turbulence model at a Reynolds number of $Re = 10^6$ and angle of attack $AoA = 6^o$. The contours of velocity magnitude in Figure (6) show a massive flow separation on the suction side of the flap starting from the shoulder region. Note that the early separation reduces the circulation around the flap and hence the lift contribution from the flap decreases rapidly.

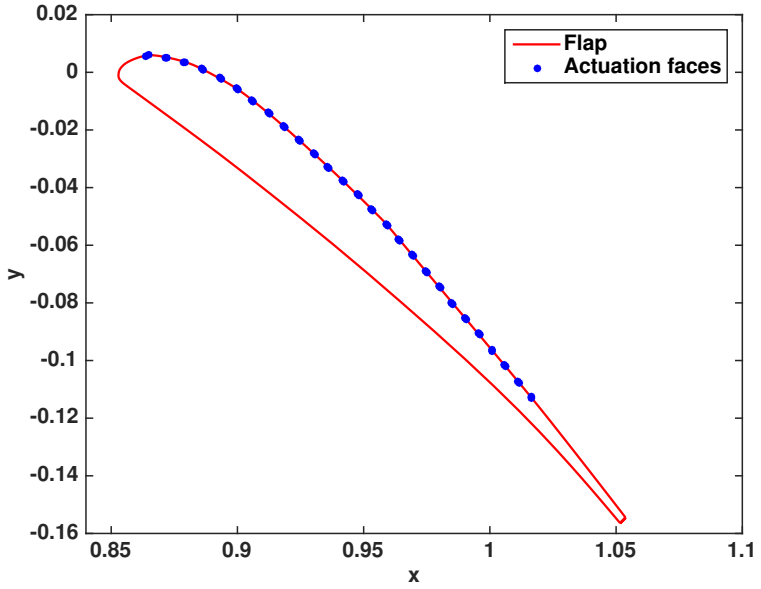

Figure 5: Actuation slot distribution on the suction side of the flap of a three-element airfoil.

In order to delay the separation and to enhance the lift coefficient of the flap, synthetic jet actuation is applied at 54 faces on the suction side of the flap. To start the optimization, initially the non-dimensional values of the actuation parameters at all the faces are chosen as $A = 0.2$, $F = 2.0$, $\beta = 90^o$ and $t_0 = -0.125$. At a blowing angle of 90^o the flow over the flap is perturbed perpendicular to the local faces. The frequency of the initial actuation is fixed to the estimated frequency of the vortex shedding of the un-actuated baseline flow. Time accurate simulations are performed with the initial control starting from a fully developed baseline flow until the non-dimensional time $T = 28$, which amounts to $40,000$ unsteady time iterations. Figure 7 shows the time history of the lift coefficient. Compared to the baseline flow with $\overline{C}_l = 2.2356$, the initial actuation has resulted in reasonable improvement in the lift coefficient with $\overline{C}_l = 2.4936$.

Our objective is to find the optimal actuation that results in maximum lift coefficient. It can be observed that the lift profile for the actuated flow shows a typical initial transient behavior, after which the flow settles down to a periodic state. For the objective function evaluation, we neglect this initial transient and compute the time-averaged lift coefficient over a sufficiently large interval of fully developed flow starting from $30,000$ time iterations to $40,000$ iterations. It can be observed that the objective function interval consists of around 14 cycles of actuation, which are good enough for a meaningful average. The discrete objective function and the corresponding Lagrangian can then be written as

$$\begin{aligned} J = \overline{C}_l &= \frac{1}{10,000} \sum_{n=30,001}^{40,000} C_l^n \left(\boldsymbol{U}^n, \boldsymbol{\alpha}\right) \\ L &= \frac{1}{10,000} \sum_{n=30,001}^{40,000} C_l^n - \sum_{n=1}^{40,000} \left[\left(\overline{\boldsymbol{U}}^n\right)^T \left(\boldsymbol{U}^n - \boldsymbol{G}^n\right) \right] \end{aligned} \tag{7}$$

The control variables are the actuation amplitudes, blowing angles and phase shifts at 54 actua-

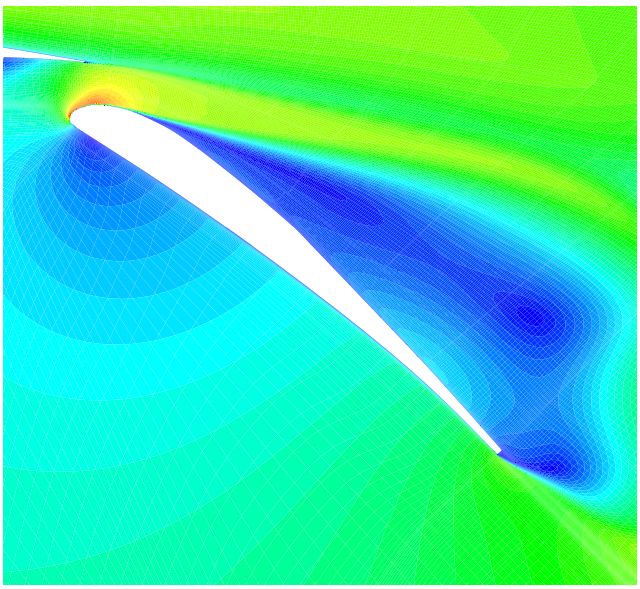

Figure 6: Baseline flow: Contours of the velocity magnitude on the flap of the three-element airfoil.

tion faces. This results in a total of 162 control variables. We now present the numerical results for optimal active flow control based on a gradient based algorithm, evolutionary algorithm and hybrid optimization approach.

5.1 Optimal Actuation based on the Gradient-based Optimization

To find the optimal actuation, the discrete adjoint URANS solver is combined with the BFGS optimization algorithm. Figure 8 shows the time-history of the lift coefficient for the optimal actuation. Compared to the un-actuated baseline flow, optimal actuation enhanced the mean lift by around 19% to a value of $\overline{C}_l = 2.6534$. Figure 9 shows the contours of velocity magnitude for the optimal case at the crest of a periodic oscillation in the lift coefficient. It can be observed that the separation point has moved further downstream of the shoulder region.

5.2 Optimal Actuation based on the Evolutionary Algorithm

Figure 8 shows the variation of the lift coefficient based on the the Evolutionary Algorithm. This approach resulted in very significant enhancement in the lift coefficient. Compared to the baseline flow, the mean lift is increased by 63% to a value of $\overline{C}_l = 3.6402$. Figure 10 shows the contours of velocity magnitude at the crest of a periodic oscillation in the lift coefficient. It can be observed that the flow is fully attached as the separation is completely suppressed.

5.3 Optimal Actuation based on the Two-level Hybrid Approach

The optimal actuation obtained from the Evolutionary Algorithm is then used as an initial condition at all the actuation faces on the suction side of the flap. Using this initial setting, the discrete adjoint URANS solver is then employed along with the BFGS algorithm to further enhance the lift coefficient. Figure 8 shows that the two-level approach has yielded a reasonable

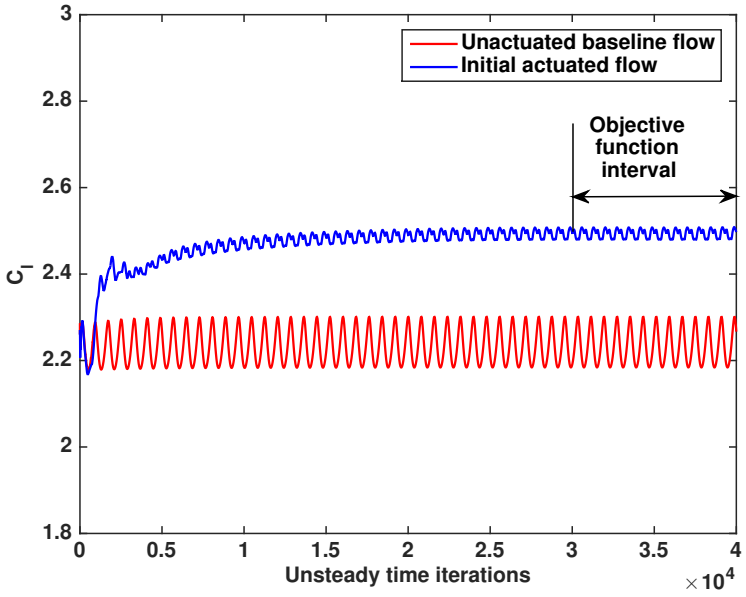

Figure 7: Comparison of the lift coefficient for the un-actuated baseline flow and the initial actuated flows.

improvement in the lift coefficient compared to Evolutionary Algorithm. The mean lift coefficient is observed to be 3.7266, which is almost 67% more than the baseline value. Figure 10 shows the corresponding contours of velocity magnitude. As a result, the two-level approach yields an improvement of the mean drag around 40% compared to the classical gradient-search. It can be concluded that, better initial values for the actuation variables, which are obtained by the global optimization brings a significant improvement as far as the optimization results are concerned. Table 1 shows a comparison of the mean-lift coefficient for the un-actuated, initial actuated and optimal actuated flows.

In the present work, the levels of the hybrid approach were only performed once such that the adjoint based gradient search stage has no effect on the initial global search using the EA. It must also be noted that the EA uses a reduced design space that is case-specific and somehow arbitrary. Therefore, choosing the reduced design space influences largely each stage's potential and emphasizes the case dependency of each stage's individual performance. More complex cases should show a stronger benefit of the hybrid algorithm.

Flow	Mean lift coefficient $\overline{C}_l$
Un-actuated baseline flow	2.2356
Initial actuated flow	2.4936
Optimal actuation based on gradient search approach	2.6534
Optimal actuation based on EA	3.6402
Optimal actuation based on hybrid approach	3.7266

Table 1: Comparison of the mean lift for the un-actuated, initial actuated and optimal actuated flows.

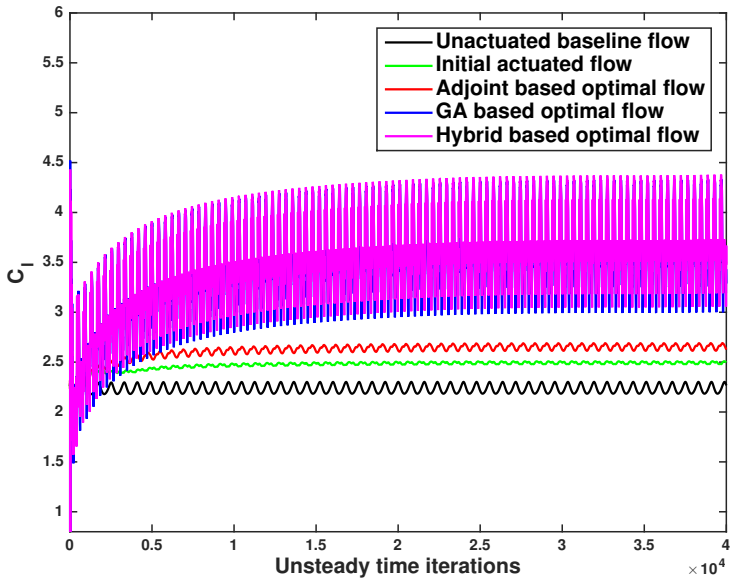

Figure 8: Comparison of the lift coefficient for the un-actuated baseline flow, initial actuated flow, optimal actuated flows based on discrete adjoint approach, evolutionary and hybrid optimization algorithms respectively.

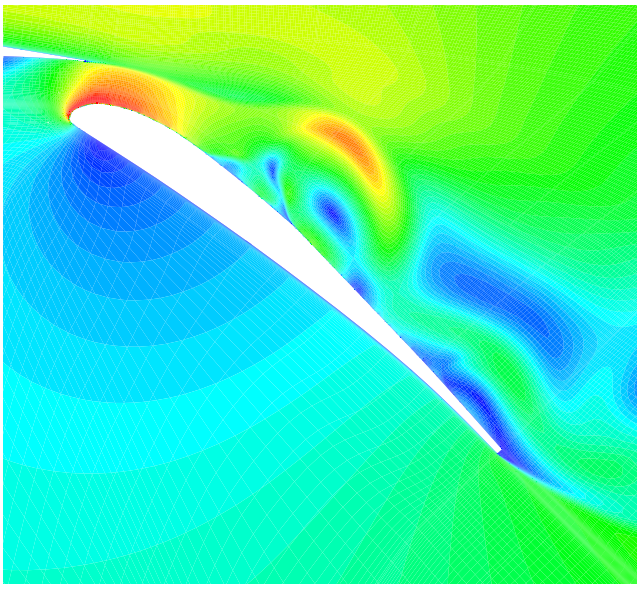

Figure 9: Optimal active flow control based on a gradient based optimization algorithm combined with discrete adjoints. Contours of the velocity magnitude on the flap of the three-element airfoil.

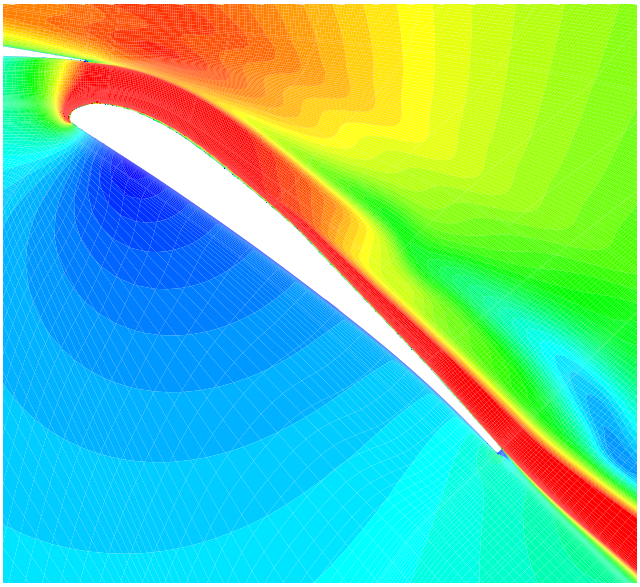

Figure 10: Optimal active flow control based on an evolutionary algorithm. Contours of the velocity magnitude on the flap of the three-element airfoil.

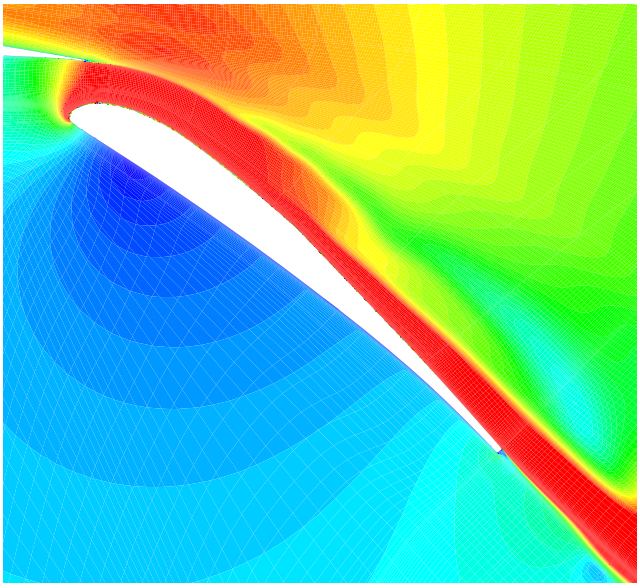

Figure 11: Optimal active flow control based on the two-level hybrid optimization algorithm. Contours of the velocity magnitude on the flap of the three-element airfoil.

6 CONCLUSIONS

In this paper, we presented a two-level approach for the optimal active flow control by combining an evolutionary algorithm based global optimization method with a gradient search method using unsteady discrete adjoints. The discrete adjoint solver for the governing incompressible URANS equations was developed by applying Algorithmic Differentiation (AD) techniques. The adjoint solver retains the full functionality of the underlying non-linear URANS solver. The suggested two-level method was then applied to find the optimal synthetic jet actuation of a three-element airfoil configuration at a Reynolds number of 10^6 and an angle of attack of 6°. Numerical results have shown that the two-level approach had yielded 67% improvement in the mean lift compared to the un-actuated baseline flow and 40% increase over the adjoint based gradient search algorithm.

ACKNOWLEDGMENTS

The authors gratefully acknowledge the computing time granted by the Allianz für Hochleistungsrechnen Rheinland-Pfalz (AHRP), Germany.

REFERENCES

[1] M. Gad-el Hak. Modern developments in flow control. *Applied Mechanics Reviews*, 49:365–379, 1996.

[2] E. Tinapp and W. Nitsche. Separation control on a high-lift configuration by periodic excitation. *Notes on Numerical Fluid Mechanics and Multidisciplinary Design (NNFM)*, 77:42–49, 2002.

[3] M. Schatz, E. Thiele, R. Petz, and W. Nitsche. Separation control by periodic excitation and its application to a high lift configuration. *AIAA Paper 2004-2507*, 2004.

[4] L. Pack, C. Yao, and A. Seifert. Application of excitation from multiple locations on a simplified high-lift system. *AIAA Paper 2004-2324*, 2004.

[5] R. Petz, W. Nitsche, M. Schatz, and F. Thiele. Increasing lift by means of active flow control on the flap of a generic high-lift configuration. *Notes on Numerical Fluid Mechanics and Multidisciplinary Design (NNFM)*, 92:257–264, 2006.

[6] M. Bauer, I. Peltzer, W. Nitsche, and B Gölling. Active flow control on an industry-relevant civil aircraft half model. *Notes on Numerical Fluid Mechanics and Multidisciplinary Design (NNFM)*, 108:95–107, 2010.

[7] B. Günther, F. Thiele, W. Petz, R. Nitsche, J. Sahner, T. Weinkauf, and H.C. Hege. Control of seperation on the flap of a three-element high-lift configuration. *AIAA paper 2007-0265*, 2007.

[8] T. Höll, A. K. V. Job, P. Giacopinelli, and F. Thiele. Numerical study of active flow control on a high-lift configuration. *Journal of Aircraft*, 49(5):1406–1422, 2012.

[9] V. Ciobaca, T. Kühn, R Rudnik, M. Bauer, B. Gölling, and W. Breitenste. Active flow-separation control on a high-lift wing-body configuration. *Journal of Aircraft*, 1:56–72, 2013.

[10] A. Seifert, T. Bachar, D. Koss, M. Shepshelovich, and I. Wyganski. Oscillatory blowing: A tool to delay boundary-layer separation. *AIAA Journal*, 31(11):2052–2060, 1993.

[11] B. L. Smith and A. Glezer. The formation and evolution of synthetic jets. *Physics of Fluids*, 10(9):2281–2297, 1998.

[12] A. Jameson, L. Martinelli, and N. Pierce. Optimum aerodynamic design using the Navier-Stokes equations. *Theor. Comput. Fluid Dyn.*, 10(1-4):213–237, 1998.

[13] A. Carnarius, B. Günther, F. Thiele, D. Wachsmuth, F. Tröltzsch, and J. C. de los Reyes. Numerical study of the optimization of separation control. *AIAA Paper 2007–58*, 2007.

[14] E. J. Nielsen and W. T. Jones. Integrated design of an active flow control system using a time-dependent adjoint method. *Mathematical Modelling of Natural Phenomena*, 6(3):141–165, 2011.

[15] A. Nemili, E. Özkaya, N. Gauger, A. Carnarius, and F. Thiele. Optimal control of unsteady flows using discrete adjoints. *AIAA Paper 2011–3720*, 2011.

[16] A. Nemili, E. Özkaya, N. Gauger, F. Kramer, A. Carnarius, and F. Thiele. Discrete adjoint based sensitivity analysis for optimal flow control of a 3D high-lift configuration. *AIAA Paper 2013–2585*, 2013.

[17] A. Griewank and A. Walther. *Evaluating derivatives: Principles and techniques of Algorithmic Differentiation*. SIAM, 2008.

[18] J. E. V. Peter and R. P. Dwight. Numerical sensitivity analysis for aerodynamic optimization: A survey of approaches and applications. *Computers & Fluids*, 39(3):373391, 2010.

[19] E. J. Nielsen and W. K. Anderson. Aerodynamic design optimization on unstructured meshes using the Navier-Stokes equations. *AIAA Journal*, 37(11):185–191, 1999.

[20] D. Quagliarella and A. Della Cioppa. Genetic algorithms applied to the aerodynamic design of transonic airfoils. *Journal of Aircraft*, 32(4):889–891, 1995.

[21] A. Oyama, S. Obayashi, and K. Nakahashi. Transonic wing optimization using genetic algorithm. *AIAA Paper 97-1854*, 1997.

[22] J. Ahn, H.-J. Kim, D.-H. Lee, and O-H. Rho. Response surface method for airfoil design in transonic flow. *Journal of Aircraft*, 38(2):231–238, 2001.

[23] M. J. D. Powell. Algorithms for approximation. chapter Radial Basis Functions for Multivariable Interpolation: A Review, pages 143–167. Clarendon Press, New York, NY, USA, 1987.

[24] Z.-H. Han, K.-S. Zhang, W.-P. Song, and Z.-D. Qiao. Optimization of active flow control over an airfoil using a surrogate-management framework. *Journal of Aircraft*, 47:603–612, 2010.

[25] J.-W. Yim, B.-J. Lee, and C. Kim. Exploring multi-stage shape optimization strategy of multi-body geometries using Kriging-based model and adjoint method. *Computers & Fluids*, 68:71 – 87, 2012.

[26] A. Nemili, E. Özkaya, N. Gauger, F. Kramer, T Höll, and F. Thiele. Optimal design of active flow control for a complex high-lift configuration. *AIAA Paper 2013–2515*, 2014.

[27] L. Hascoët and V. Pascual. The Tapenade Automatic Differentiation tool: Principles, Model, and Specification. *ACM Transactions On Mathematical Software*, 39(3), 2013.